Molecular dynamics simulations of martensitic fcc-to-hcp phase transformations in strained ultrathin metallic films

Kedarnath Kolluri, M. Rauf Gungor, and Dimitrios Maroudas*
Department of Chemical Engineering, University of Massachusetts, Amherst, Massachusetts 01003-3110, USA
(Received 24 August 2008; published 6 November 2008)

We report results of molecular dynamics simulations that reveal fcc→hcp martensitic transformations in biaxially strained ultrathin films of face-centered cubic metals. We find that martensites nucleate at the surface and grow into the bulk of the film due to dislocation glide; in this process, the magnitudes of the relative atomic slip displacements are identical to those proposed for Bain transformations. Mechanical stability analysis shows that the onset of the phase transformation is consistent with the onset of a shearing instability of the thin film.

DOI: 10.1103/PhysRevB.78.195408 PACS number(s): 64.70.Nd, 64.70.kd, 81.30.Hd, 81.30.Kf

I. INTRODUCTION

Structural transformations in steel during rapid cooling from high temperatures lead to hardening and strengthening of the material. Deforming the material at shock-loading rates may have similar effects on its mechanical properties. Such structural transitions, known as martensitic transformations, have been studied for over 100 years in ferrous alloys and other metals. A martensitic transformation is a stress-driven diffusionless structural phase transition that occurs through collective atomic motion.[1,2] Martensite phases can nucleate both homogenously, when the bulk material is subjected to high temperature and/or pressure or stress, and heterogeneously at lattice defects. Martensitic transformations have been exploited to improve the strength of alloys and ceramics[1–3] and to design shape memory alloys,[4] as well as various microscale and nanoscale devices.[5] Such transformations occur even in biological systems.[6] Homogeneously nucleated martensitic transformations in bulk materials subjected to high pressure and temperature have been studied both experimentally[1,2] and theoretically.[7–10] However, the study of heterogeneous nucleation of martensite phases has been limited. Heterogeneous nucleation is most commonly observed in thin films of pure metals and alloys due to the prevalence of heterogeneous nucleation sites, such as surfaces and interfaces.[11–14]

In experimental studies of structural transitions in thin films of various materials, it was found that substrate-induced stress can cause martensitic transformations[11] and that stacking faults play a dominant role in these transformations even under shock-loading conditions.[12,13] Experimental studies also suggest that the occurrence of martensitic transformations depends on the crystallographic orientation of the film surface[15] and that martensitic transitions can cause thin-film surface roughening.[16] In spite of these advances, however, a fundamental understanding of the martensitic transition mechanisms and the implications of these transformations for thin-film properties and function remain elusive. Such a fundamental understanding of structural response is required in predicting the mechanical behavior of metallic thin films that are widely used in nanotechnological applications,[17] as well as in microelectromechanical and nanoelectromechanical systems engineering.[5] In this paper, we report an atomic-scale analysis, which is based on large-scale molecular dynamics (MD) simulations, of martensitic transformations from a face-centered cubic (fcc) to a hexagonal close-packed (hcp) phase in ultrathin (a few nanometers thick) Cu films with $[1\bar{1}0]$ surface orientation that have been strained biaxially at shock-loading strain rates. Our simulations reveal that at high levels of applied tensile strain, the martensite phase is nucleated heterogeneously at the thin-film surface and grows into the bulk of the film due to the propagation of stacking faults caused by the glide motion of partial dislocations that bound the faults. Consistently with recent experimental findings,[11–16] our simulation results emphasize and elucidate the important role of stacking faults and surface crystallographic orientation in facilitating martensitic transformations of metallic thin films under shock-loading conditions. The transition onset and the orientation relationship between the parent and the martensite phase are consistent with the onset of a shear instability in the $(001)_{fcc}$ crystallographic plane.

This paper is structured as follows. The interatomic interactions in the metallic films used in our study, as well as the computational methods employed in our molecular dynamics simulations and the analysis of the simulation results are described and discussed in Sec. II. In Sec. III, the simulation results are presented and the observed martensitic transformations are analyzed systematically and are also discussed from the viewpoint of the films mechanical stability. To verify our predictions and validate the statements made based on our analysis, we have carried out calculations employing two different interatomic interaction potentials; the most important comparisons of the predictions of the two potentials, in the context of martensitic transformation, are presented in Sec. IV. Finally, the main conclusions of our study are summarized in Sec. V.

II. MOLECULAR DYNAMICS SIMULATIONS

We studied the response of freestanding ultrathin fcc metallic films to applied biaxial tension through isothermal-isostrain MD simulations at $T=100$ K; the model and methods employed have been discussed in Ref. 18. Specifically, the interatomic interactions were described according to the

embedded-atom-method (EAM) potential for Cu developed by Oh and Johnson.[19] In this EAM parametrization, the total energy of the fcc lattice under uniform compression and dilation is required to obey the universal equation of state proposed by Rose *et al.*[20] As a result, the EAM potential accounts properly for the lattice anharmonicity[21] and provides a good modeling framework for simulating high-pressure and shock-loading experiments.[20,21] The potential has been tested extensively regarding its predictions of structural and mechanical properties.[22] To verify further the reproducibility of our results and robustness of our statements, we have repeated our calculations with a second EAM potential for Cu that was parametrized by Mishin *et al.*[23] by explicitly fitting to the generalized stacking fault energy of Cu; here, we refer to this potential as EAM-Mishin. The results that we obtained using both of these potentials were in excellent qualitative and very good quantitative agreement. The most important of these comparisons are presented in Sec. IV.

We used slab supercells with free surfaces in the z direction; the Cartesian x, y, and z axes were taken along the [111], $[\bar{1}\bar{1}2]$, and $[1\bar{1}0]$ crystallographic directions, respectively, and the surface plane was the $(1\bar{1}0)$ crystallographic plane. The simulation cells examined contained 1 272 000 (576 000) atoms with cell dimensions of $L_x \times L_y \times L_z = 56.35 \times 53.13 \times 5.11$ nm^3 ($37.57 \times 35.42 \times 5.11$ nm^3) in the unstrained state. The thin films were strained biaxially by expanding the supercell uniformly along x and y up to a chosen strain level, ε, at the rate of 3×10^{11} s^{-1}, and then isostrain conditions were maintained during structural relaxation (the strain components $\varepsilon_{xx} = \varepsilon_{yy} = \varepsilon$; ε_{zz} was not controlled). The responses of both the smaller and the larger films were found to be identical and the atomistic mechanisms identified were not affected by the strain rate over a one-order-of-magnitude range examined. Point and line defects in the films were identified by calculating the atomic coordination numbers and by conducting common neighbor analysis[24] in order to identify atoms in locally perfect hcp and fcc lattice arrangements. The public-domain computer software ATOMEYE was used for visualization of the MD-generated atomic configurations.[25]

III. MARTENSITIC TRANSFORMATION AND STABILITY ANALYSIS

Our MD simulations reveal that for applied biaxial strains, $\varepsilon > 5\%$, structural relaxation in the thin films occurs through the nucleation and glide of Shockley partial dislocations and threading dislocation loops, which lead to formation of stacking faults; these faults are identified as atoms arranged locally in a perfect hcp lattice. The percentages of different types of atoms in the thin films are plotted in Fig. 1(a) as a function of ε after steady state has been reached at each strain level examined. The steep increase in the percentage of hcp atoms for $\varepsilon \geq 10\%$ demonstrates the structural transition of the Cu thin film from a fcc to a hcp lattice. The top views of the thin films subjected to applied biaxial strains $\varepsilon = 9\%$ and 12% are shown in the insets of Fig. 1(a) and highlight the difference in the structural response to the different levels of ε; the top view of the thin film under ε

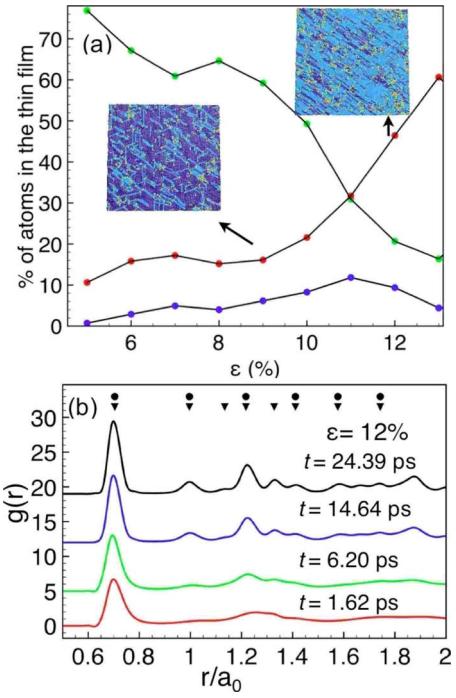

FIG. 1. (Color online) (a) Dependence on the applied biaxial strain, ε, of the percentages of various kinds of atoms in strain-relaxed thin films at $t = 32.48$ ps, where the MD simulation time, t, is recorded starting from the film at its unstrained state. Blue solid circles denote percentages of structural defects, while red and green solid circles denote percentages of atoms in hcp and fcc lattice arrangements, respectively. The insets show the top views of the strain-relaxed thin films subjected to applied biaxial strains $\varepsilon = 9\%$ and 12%; the surface plane is the $(1\bar{1}0)$ plane. Atoms in locally perfect fcc and hcp environments are colored dark and light blue, respectively, while the remaining colored atoms are inside dislocation cores. Surface atoms are not shown for clarity. (b) Evolution (shown by upward shifting) of the pair-correlation function, $g(r)$, during the strain relaxation of a Cu thin film with a fcc lattice structure initially strained biaxially to $\varepsilon = 12\%$. Solid triangles and circles indicate peak positions in the $g(r)$ that correspond to the sequence of coordination shells in perfect fcc and hcp crystals, respectively, and $a_0 = 3.615$ Å is the equilibrium lattice parameter of fcc Cu. The absence of sharp peaks in the early $g(r)$ of the fcc film is due to a disordering of the fcc lattice as a result of straining at shock-loading rates.

$= 12\%$, which has undergone a fcc $\rightarrow$ hcp transformation, resembles (very closely) that of experimentally observed martensites.[11–16,26] Martensitic transformations induced by thermal or mechanical strains have been observed in experimental studies at moderate ($1 \times 10^2 - 1 \times 10^3$ s^{-1}) and high ($> 1 \times 10^6$ s^{-1}) strain rate deformations of 304L stainless steel.[13] Moreover, heterogeneous martensitic transformations induced by plastic deformation have also been reported in experimental studies where shock loading was applied through ball milling[12] or by conducting shock-recovery experiments.[14] This fcc $\rightarrow$ hcp transition is most evident from the evolution of the pair-correlation function, $g(r)$, shown in Fig. 1(b) during the strain relaxation of a Cu thin film with a fcc lattice structure initially, after it has been strained biaxially to $\varepsilon = 12\%$. For example, an unambiguous indication of

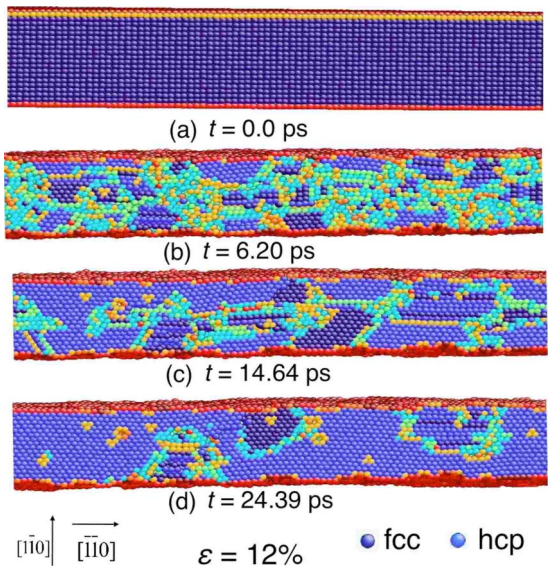

FIG. 2. (Color online) [(a)–(d)] A cross-sectional view of a biaxially strained (to $\varepsilon=12\%$) Cu thin film showing the evolution of the film structure as it undergoes structural transition from an initial fcc lattice [(a)]; the plane shown is the (001) fcc lattice plane. Dark and light blue atoms are in perfect fcc and hcp lattice arrangements, respectively. Maroon and other colored atoms are on the surface and inside dislocation cores, respectively. The three subdomains shown in (d) that are embedded in the hcp-martensite phase are faulted hcp (middle) and fcc regions.

the fcc→hcp transition is the appearance of the third and fifth peaks in the $g(r)$ curve shown in black, which is characteristic of a hcp lattice. The resulting hcp Cu has a lattice-parameter ratio of $c/a=1.612$, i.e., very close to that of the perfect hcp lattice, $(8/3)^{1/2}$. We conclude that structural relaxation after biaxial tensile straining to $\varepsilon \geq 10\%$ results in a martensitic fcc→hcp transformation.

Figure 2 shows a cross-sectional view of the structural evolution during strain relaxation of the thin film that has been strained biaxially to $\varepsilon=12\%$; the plane shown corresponds to the (001) crystallographic plane of the original fcc phase, $(001)_{\text{fcc}}$. This evolution sequence shows the film as it undergoes structural transition from its initial fcc lattice. After the biaxial straining of the film and during the subsequent structural relaxation at isostrain conditions ($\varepsilon=12\%$), multiple partial dislocation loops are emitted simultaneously from the film surface and glide in successive {111} slip planes along ⟨112⟩ directions; these loops have Burgers vectors $(a/6)\langle 112\rangle$ where a is the fcc lattice parameter. The glide of these loops in successive atomic planes is analogous to twinning mechanisms that are observed commonly in fcc metals[27] and leads to the nucleation of a shear-induced hcp phase near the film surface [Fig. 2(b)]. The martensite then propagates and the hcp phase grows as the dislocation loops extend into the bulk of the film [Figs. 2(c) and 2(d)]. The $(001)_{\text{fcc}}$ plane [Fig. 2(a)] now corresponds to the $(0001)_{\text{hcp}}$ plane [Fig. 2(d)], i.e., the basal plane of the hcp lattice structure. The habit plane of the heterogeneously nucleated $(001)_{\text{fcc}}\|(0001)_{\text{hcp}}$ structural transition, i.e., an invariant crystallographic plane common to both the parent lattice and the martensite, was found to be normal to the $[1\bar{1}0]_{\text{fcc}}$ direction and parallel to the original film surface plane.

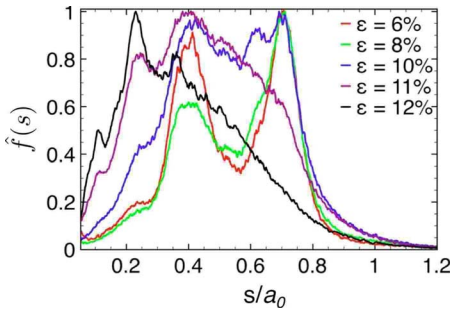

FIG. 3. (Color online) Dependence on ε of the distribution $\hat{f}(s)$ of the relative slip vector magnitudes in strain-relaxed thin films at $t=32.48$ ps.

Martensitic transformations of the $(001)_{\text{fcc}}\|(0001)_{\text{hcp}}$ type have also been observed in large-scale MD simulations of shock loading of body-centered cubic (bcc) metals[8] and have been analyzed in a recent first-principles study.[10] In those studies, however, the martensite was found to be nucleated homogeneously. In addition, in the study in Ref. 10, the transformation mechanism involved slip of (001) planes and an intermediate orthorhombic state, which is not observed in our MD simulations. Our analysis reveals that the martensitic transformation in biaxially strained thin films is mediated by plastic deformation. The structural evolution depicted in Fig. 2 shows that the transformation is facilitated by the dislocation glide motion and the martensite phase grows due to the propagation of the stacking faults bounded by these partial dislocations. Furthermore, in our earlier MD simulations of strain relaxation in biaxially strained thin metallic films with [111]-oriented free surfaces, martensitic transformations were not observed.[18] In this study, the low symmetry of the $(1\bar{1}0)_{\text{fcc}}$ surface plane limits the availability of the ⟨110⟩{111} and ⟨112⟩{111} slip systems and leads to nucleation of line defects in successive $\{111\}_{\text{fcc}}$ slip planes, which facilitates the martensitic transformation.

We have analyzed the magnitudes of the atomic displacements for the atoms in the structurally transformed thin film that have undergone slip relative to their neighbors in the unstrained fcc state, which is taken as the reference configuration. The slip vector of an atom, α, in the thin film is given by $\mathbf{s}^{\alpha}=-(1/n_s)\Sigma_{\beta\neq\alpha}^{n_s}\mathbf{x}^{\alpha\beta}-\mathbf{X}^{\alpha\beta}$, where $\mathbf{x}^{\alpha\beta}$ and $\mathbf{X}^{\alpha\beta}$ are the distance vectors between atoms α and β (from α to β) in their current and reference configurations, respectively, and n_s is the number of neighbors of atom α that have undergone slip;[28] in our analysis, we consider the atom α to have slipped with respect to atom β if $|\mathbf{x}^{\alpha\beta}-\mathbf{X}^{\alpha\beta}|>0.4$ Å. In Fig. 3, distributions of the slip vector magnitudes, $s\equiv|\mathbf{s}|$, of all the atoms that have slipped in strain-relaxed thin films for various strain levels, ε, are plotted. Specifically, the function $\hat{f}(s)=f(s)/[f(s)]_{\max}$ is plotted, where $\int_{s>0}f(s)ds=N_{\text{slipped}}$ and N_{slipped} is the total number of atoms in the thin film that have undergone slip displacements. For $\varepsilon<10\%$, the $\hat{f}(s)$ distributions are centered at the Burgers vector magnitude, b, of perfect and Shockley partial dislocations, $b=a/\sqrt{2}$ and $a/\sqrt{6}$, respectively. For $\varepsilon>10\%$, we observe a shift in these distributions, which become centered at $a\sqrt{2}/6$ and $a/\sqrt{6}$.

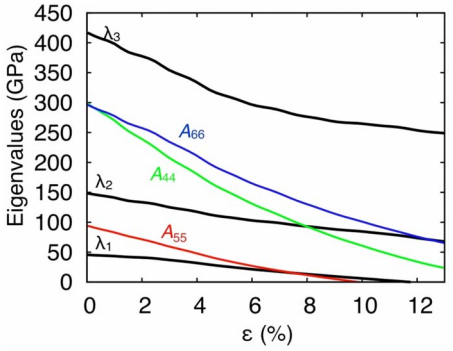

FIG. 4. (Color online) Eigenvalues of the symmetrized elastic stiffness moduli matrix, **A**, as a function of ε, as calculated immediately after the application of the biaxial strain.

The relative slip vector magnitude that we found in our analysis, $a\sqrt{2}/6$, is consistent with the atomic displacements proposed in the theoretical study of Dmitriev *et al.*,[29] which provided a unified theoretical framework for the description of the Burgers and Bain mechanisms of bcc→hcp and bcc→fcc transformations, respectively. In both cases, the corresponding relative displacement magnitudes are equal to $a\sqrt{2}/6$. The fcc→hcp transformation can be considered as a combination of the Bain and the Burgers mechanisms (fcc→bcc+bcc→hcp), and therefore, the corresponding relative displacement magnitude should also be $a\sqrt{2}/6$. Nevertheless, in our simulations, these displacements are a result of dislocations gliding in successive atomic planes as opposed to concerted motion of adjacent atomic planes in opposite directions (as in the Burgers mechanism) or in the same direction (as in the Bain deformation). The beginning of the shift in the distributions of Fig. 3 marks the onset of the martensitic transformation.

We carried out mechanical stability analysis[30,31] in order to predict the loss of the crystalline fcc lattice stability under the conditions of our simulations. The analysis revealed that shear, as well as Born instabilities are triggered prior to the martensitic transformation in our metallic thin-film models. Specifically, we calculated the modes of destabilization of the symmetrized version, $\mathbf{A}=(1/2)(\mathbf{B}+\mathbf{B}^T)$, of the elastic stiffness moduli matrix, **B**.[31] Given that the habit plane is $(1\bar{1}0)_{\mathrm{fcc}}$, we transformed **B** from the original coordinate system to one with coordinate axes x', y', and z' that are taken along the [110], [001], and $[1\bar{1}0]$ crystallographic directions, respectively. The form taken by matrix **A** implies that the conditions for the stability of the fcc lattice are $\det(\mathbf{A}_m)>0$, $A_{44}>0$, $A_{55}>0$, and $A_{66}>0$, where the elements of matrix **A** are expressed in contracted Voigt notation and $\mathbf{A}_m$ is the 3×3 matrix $[A_{ij};\ i,j=1,2,3]$. We denote the real and positive eigenvalues of $\mathbf{A}_m$ by λ_1, λ_2, and λ_3, with $\lambda_1<\lambda_2<\lambda_3$.

The eigenvalues of matrix **A**, λ_1, λ_2, λ_3, $\lambda_4=A_{44}$, $\lambda_5=A_{55}$, and $\lambda_6=A_{66}$, are plotted in Fig. 4 as a function of ε. For each value of ε, the elements of **A** were computed immediately after the application of the biaxial strain, i.e., at the end of the dynamic straining period to bring the film from its unstrained state to this strain state, ε. Figure 4 shows the onset of a shear instability in the (001) crystallographic plane associated with the vanishing of A_{55} ($A_{55}=A_{x'z'x'z'}=0$) occurring at a strain $\varepsilon\sim10\%$. In the MD simulations, for $\varepsilon=10\%$, we observe the nucleation at the surface of the Cu thin film of isolated hcp-martensite embryos, most of which do not extend into the bulk of the film. The MD simulations also reveal that martensite grains continue to nucleate and grow with increasing applied strain (e.g., $\varepsilon=11\%$). The Born instability, associated with the vanishing of λ_1 ($\lambda_1=0$), occurs at $\varepsilon\sim12\%$ and leads to the breaking of the fcc lattice symmetry. This bifurcation, the onset of the Born instability, also causes the material to transform to a new stable lattice structure, which is the hcp phase. The bifurcation, in conjunction with the driving force provided by the applied strain, leads to the growth of martensite embryos into the bulk of the film and completes the structural transition [Fig. 2(d)]; in this state, the hcp phase has grown throughout the film thickness and the film is predominantly hcp martensite. We conclude that the breaking of the fcc lattice symmetry in the thin film marks the onset of martensitic transformation, which is mediated by plastic deformation.

IV. COMPARISON OF PREDICTIONS OF TWO INTERATOMIC POTENTIALS

The MD simulations and analysis presented in Sec. III were based on a description of interatomic interactions in Cu according to the Oh and Johnson potential.[19] To demonstrate the reproducibility of our results and validate our analysis and the statements made in Sec. III, we have compared our MD simulation results and mechanical stability analysis according to the Oh and Johnson potential (Sec. III) with those obtained by using the EAM-Mishin potential.[23] The choice of the EAM-Mishin potential for this comparison is due to the excellent attributes of this potential in modeling Cu mechanical behavior. Importantly, the EAM-Mishin potential was developed by fitting specifically the EAM model to the experimentally determined stacking fault energy of Cu (45 $\mathrm{mJ/m^2}$); the stacking fault energy predicted by the EAM-Mishin potential is 44.4 $\mathrm{mJ/m^2}$.[23] Zhu *et al.*[32] verified further the ability of the EAM-Mishin potential to predict accurately the characteristics of the first nucleated dislocation in nanoindentation experiments; in particular, the potential predicted the mixed shear mode of the Shockley partial in nanoindentation simulations. In addition, we found that the predictions of the Oh and Johnson potential are in very good agreement with those of *ab initio* calculations and EAM-Mishin for the stress-strain curves of Cu shearing deformation in the [111] plane along the $[11\bar{2}]$ direction.

Figure 5 shows the eigenvalues λ_1 and A_{55} of matrix **A** for biaxially strained copper; as shown in Sec. III, these are the eignevalues of **A** that go to zero first as the biaxially applied tensile strain increases. The results for thin films that are modeled according to the Oh and Johnson and EAM-Mishin EAM parametrizations for copper are shown in Figs. 5(a) and 5(b), respectively. By comparison of the results in Figs. 5(a) and 5(b), it is evident that the mechanical instabilities predicted by the EAM-Mishin potential are in very good agreement with the predictions of the Oh and Johnson potential: the agreement is excellent qualitatively (in terms of the

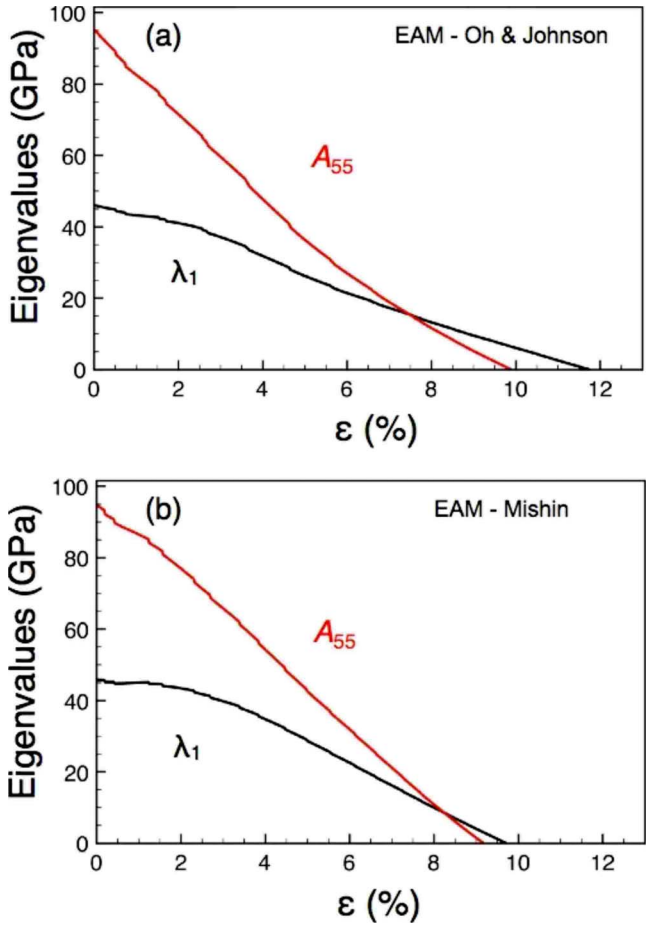

FIG. 5. (Color online) The two eigenvalues of the symmetrized elastic stiffness moduli matrix **A** that go to zero first, λ_1 and A_{55}, signifying the key modes of instability for biaxially strained thin films modeled according to the (a) Oh and Johnson (Ref. 19) and (b) EAM-Mishin (Ref. 23) potentials.

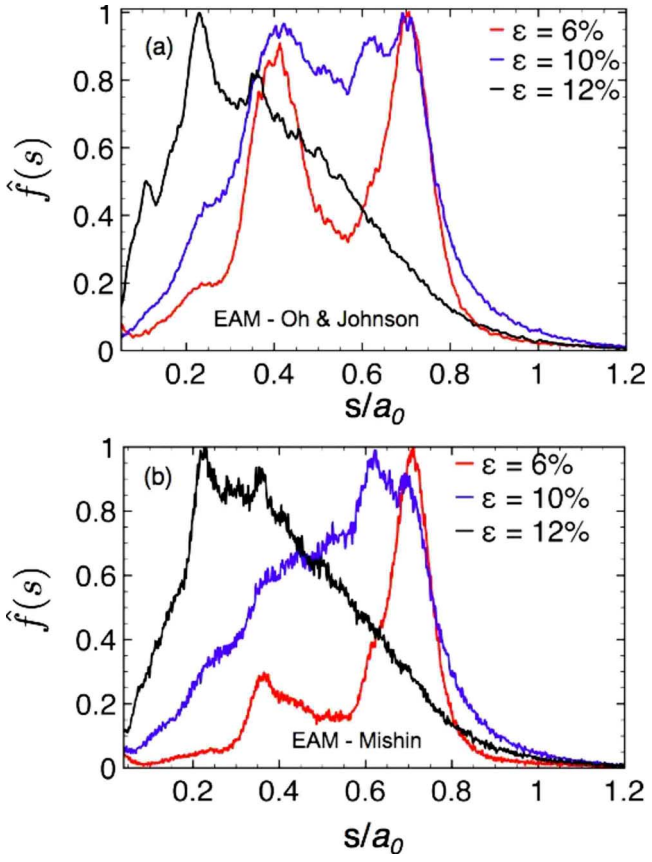

FIG. 6. (Color online) Distributions of the relative slip vector magnitudes, $\hat{f}(s)$, for different applied biaxial strains, ε, for thin films modeled with (a) the Oh and Johnson (Ref. 19) and (b) the EAM-Mishin (Ref. 23) potentials for copper.

variation with strain and the order that the eigenvalues "cross zero") and very good quantitatively.

Finally, the distribution of the relative slip vector magnitudes for copper thin films biaxially strained to various strain levels are plotted in Fig. 6. Figures 6(a) and 6(b) show the distributions predicted based on the Oh and Johnson and EAM-Mishin potentials, respectively. Both EAM parametrizations predict the exact same shifts in the centers of the distributions of slip vector magnitudes for all the atoms that have undergone slip, $\hat{f}(s)$, from Burgers vector magnitudes, b, of perfect and Shockley partial dislocations, $b=a/\sqrt{2}$ and $a/\sqrt{6}$, respectively, for $\varepsilon<10\%$ to $a\sqrt{2}/6$ and $a/\sqrt{6}$, and for $\varepsilon>10\%$; therefore, the two potentials are in excellent qualitative agreement in their predictions of the distribution shifts with strain level ε for strain-relaxed films. The relative magnitudes of the peaks corresponding to the partial dislocations and perfect dislocations, however, are not the same when comparing simulation results based on the two different potentials. We attribute these differences to the differences in the stacking fault energies predicted by the two potentials.

Based on the above comparisons, we conclude that the predictions of the Oh and Johnson Cu potential regarding thin-film mechanical behavior and martensitic transformation presented in Sec. III are reliable. These comparisons validate our analysis and the statements made in Sec. III, based on the analysis.

V. SUMMARY

In summary, we carried out a systematic atomic-scale analysis of fcc→hcp martensitic transformations in nanometer-scale-thick Cu films with $[1\bar{1}0]$ surface crystallographic orientation. The analysis was based on molecular dynamics simulations of film biaxial tensile straining at shock-loading conditions followed by structural relaxation under isostrain conditions. Our simulations revealed that martensitic phase transformations occur at high levels of applied strain. More importantly, the martensite phase was found to nucleate heterogeneously at the thin-film surface and subsequently grow into the bulk of the film; the growth process is mediated by the propagation of stacking faults, which is caused by partial dislocation glide motion. Our results are consistent with recent experimental findings and emphasize the important role of surface crystallographic orientation in the occurrence of martensitic transformations in strained thin films. The results also elucidate the role of stacking faults in facilitating such martensitic transformations in fcc metallic thin films. Our analysis is also consistent

with and supports (from a computer-simulation point of view) recent theoretical studies, which have elucidated the emergence of lattice defects in reconstructive transformations, such as the fcc→hcp martensitic transformations, as well as close-to-reconstructive transformations.[33] Moreover, the microstructures observed in our simulations are very similar to those observed in experimental studies,[11–16] which support that the transformation mechanisms identified by the MD simulations are consistent with the mechanisms that are operative in the experiments. Finally, our mechanical stability analysis showed that the orientation relationship between the parent and the martensite phase and the onset of the phase transformation are consistent with the onset of a shear instability in the thin film.

The fundamental understanding of martensitic transformations in metallic fcc thin films under high levels of applied biaxial strain provided by our analysis can have important implications for the mechanical reliability of thin films that are used widely in microelectronic devices and nanofabrication technologies. Such a fundamental mechanistic understanding and modeling predictions may enable improved designs of nanoelectromechanical systems.

ACKNOWLEDGMENTS

Fruitful discussions with H. Djohari and F. Milstein are gratefully acknowledged. This work was supported by the Office of Basic Energy Sciences, U.S. Department of Energy through Grant No. DE-FG02-07ER46407.

*Corresponding author: maroudas@ecs.umass.edu

[1] H. K. D. H. Bhadeshia, in *Encyclopedia of Materials Science: Science and Technology*, edited by K. H. J. Buschow, R. Cahn, M. C. Flemings, B. Ilschner, E. J. Kramer, S. Mahajan, and P. Veyssiere (Pergamon, New York/Elsevier Science, New York, 2001), p. 5203.

[2] *Martensite*, edited by G. B. Olson and W. Owen (ASM International, Materials Park, OH, 1992).

[3] M. H. Bocanegra-Bernal and S. D. De la Torre, J. Mater. Sci. **37**, 4947 (2002).

[4] R. D. James and M. Wuttig, Philos. Mag. A **77**, 1273 (1998); A. Sozinov, A. A. Likhachev, N. Lanska, and K. Ullakko, Appl. Phys. Lett. **80**, 1746 (2002).

[5] K. Bhattacharya and R. D. James, Science **307**, 53 (2005).

[6] G. B. Olson and H. Hartman, J. Phys. Colloq. **43**, 855 (1982).

[7] P. Entel, R. Meyer, K. Kadau, H. C. Herper, and E. Hoffmann, Eur. Phys. J. B **5**, 379 (1998).

[8] K. Kadau, T. C. Germann, P. S. Lomdahl, and B. L. Holian, Science **296**, 1681 (2002).

[9] J. H. Zhao, D. Maroudas, and F. Milstein, Phys. Rev. B **62**, 13799 (2000); F. Milstein, J. H. Zhao, and D. Maroudas, *ibid.* **70**, 184102 (2004).

[10] E. Kim, M. Nicol, H. Cynn, and C. S. Yoo, Phys. Rev. Lett. **96**, 035504 (2006).

[11] Y. Liu and X. Huang, Philos. Mag. **84**, 1919 (2004).

[12] J. Sort, S. Suriñach, J. S. Muñoz, M. D. Baró, M. Wojcik, E. Jedryka, S. Nadolski, N. Sheludko, and J. Nogués, Phys. Rev. B **68**, 014421 (2003).

[13] See, e.g.,W.-S. Lee and C.-F. Lin, Scr. Mater. **43**, 777 (2000), and references therein.

[14] L. L. M. Hsiung, *Linking Length Scales in the Mechanical Behavior of Materials*, MRS Symposia Proceedings No. 882E (Materials Research Society, Pittsburgh, 2005), p. E.E4.8.1.

[15] H. T. Hesemann, P. Müllnerb, O. Kraft, D. Nowak, S. P. Baker, K. Finkelstein, and E. Arzt, Scr. Mater. **48**, 1129 (2003).

[16] J. Espinosa, H. Shi, and D. Lederman, J. Appl. Phys. **99**, 023516 (2006).

[17] W. D. Nix, Metall. Trans. A **20A**, 2217 (1989).

[18] M. R. Gungor and D. Maroudas, J. Appl. Phys. **97**, 113527 (2005); Appl. Phys. Lett. **87**, 171913 (2005); K. Kolluri, M. R. Gungor, and D. Maroudas, *ibid.* **90**, 221907 (2007); J. Appl. Phys. **103**, 123517 (2008).

[19] D. J. Oh and R. A. Johnson, J. Mater. Res. **3**, 471 (1988); R. A. Johnson, Phys. Rev. B **37**, 3924 (1988).

[20] J. H. Rose, J. R. Smith, F. Guinea, and J. Ferrante, Phys. Rev. B **29**, 2963 (1984).

[21] S. M. Foiles and M. S. Daw, Phys. Rev. B **38**, 12643 (1988).

[22] J. A. Zimmerman, H. Gao, and F. F. Abraham, Modell. Simul. Mater. Sci. Eng. **8**, 103 (2000).

[23] Y. Mishin, M. J. Mehl, D. A. Papaconstantopoulos, A. F. Voter, and J. D. Kress, Phys. Rev. B **63**, 224106 (2001).

[24] J. D. Honeycutt and H. C. Andersen, J. Phys. Chem. **91**, 4950 (1987).

[25] J. Li, Modell. Simul. Mater. Sci. Eng. **11**, 173 (2003).

[26] See, e.g., T. Waitz and H. P. Karnthaler, Acta Mater. **45**, 837 (1997); A. D. J. Saldívar García, A. M. Medrano, and A. S. Rodriguez, Metall. Mater. Trans. A **30**, 1177 (1999).

[27] See, e.g., V. Yamakov, D. Wolf, S. R. Phillpot, A. K. Mukherjee, and H. Gleiter, Nature Mater. **1**, 45 (2002).

[28] J. A. Zimmerman, C. L. Kelchner, P. A. Klein, J. C. Hamilton, and S. M. Foiles, Phys. Rev. Lett. **87**, 165507 (2001).

[29] V. P. Dmitriev, Yu. M. Gufan, and P. Tolédano, Phys. Rev. B **44**, 7248 (1991).

[30] J. H. Wang, J. Li, S. Yip, S. R. Phillpot, and D. Wolf, Phys. Rev. B **52**, 12627 (1995).

[31] J. W. Morris, Jr. and C. R. Krenn, Philos. Mag. A **80**, 2827 (2000).

[32] T. Zhu, J. Li, K. J. Van Vliet, S. Ogata, S. Yip, and S. Suresh, J. Mech. Phys. Solids **52**, 691 (2004).

[33] See e. g., F.-J. Perez-Reche, L. Truskinovsky, and G. Zanzotto, Phys. Rev. Lett. **99**, 075501 (2007); K. Bhattacharya, S. Conti, G. Zanzotto, and J. Zimmer, Nature (London) **428**, 55 (2004).